Excitations of nanoscale quantum liquids under pressure and the Bose glass phase

Jacques Bossy,[1] Jonathan V. Pearce,[2,3,*] Helmut Schober,[3] and Henry R. Glyde[2]
[1]*Institut Néel, CNRS-UJF, BP 166, 38042 Grenoble Cedex 9, France*
[2]*Department of Physics and Astronomy, University of Delaware, Newark, Delaware 19716-2570, USA*
[3]*Institut Laue-Langevin, BP 156, 38042 Grenoble Cedex, France*
(Received 22 July 2008; published 5 December 2008)

We present neutron scattering measurements of the dynamic structure factor of liquid helium confined to nanoscales in 25 and 34 Å mean pore diameter porous media over a range of pressures and temperatures. At low temperature and low pressure we observe well-defined phonon-roton (P-R) modes characteristic of liquid helium containing Bose-Einstein condensation (BEC). As pressure is increased above 25 bars, we observe that the high energy P-R modes broaden and become unobservable. At pressure $p=36.3-36.8$ bars we observe loss of all modes, including the roton. The observation of modes up to 36.3–36.8 bars indicates that there is liquid containing BEC in the gelsils up to this pressure. The loss of modes at 36.3–36.8 bars indicates loss of BEC in the liquid or significant solidification in the gelsils at this pressure. At a pressure of 31.2 bars, we observe well-defined P-R modes up to $T\simeq 1.4$ K but loss of all modes above this temperature. At $p\simeq 0$, we have previously observed modes up to $T_\lambda=2.17$ K. Yamamoto *et al.* have reported superfluidity in the same 25 Å gelsil up to a pressure $p_c=34$ bars at $T\simeq 0$ K and to a maximum temperature of $T_c=1.3$ K at $p\simeq 0$. The transition at $p_c=34$ bars and $T\simeq 0$ K was interpreted as a quantum phase transition. The present observation of P-R modes at temperatures well above T_c (and pressures slightly above p_c) indicates that there is a phase containing BEC above T_c (p_c) that is not superfluid. This is interpreted as a Bose glass phase containing islands of BEC that support P-R modes separated by normal liquid so that there is no phase coherence across the sample as needed for superflow. The Bose glass phase lies between the superfluid and normal liquid at all temperatures and pressures. Measurements of the static structure factor indicate that freezing in the gelsils is predominantly to an amorphous solid.

DOI: 10.1103/PhysRevB.78.224507 PACS number(s): 67.25.dj, 61.05.fg

I. INTRODUCTION

There is currently fresh interest in exploring the properties of liquid helium under pressure, both bulk liquid helium[1–4] and helium confined in porous media.[5–11] The goal is essentially to reveal and understand Bose-Einstein condensation (BEC) and superfluidity in dense Bose liquids, again both in uniform liquids and liquids confined to nanoscales and in disorder. Interest is also stimulated by the observation[12–16] of a possible superfluid phase in solid helium and similarities between the solid and liquid.

^{4}He in porous media[17] is also an example of bosons in disorder,[18–24] as are Cooper pairs (bosons) in high T_c superconductors[25,26] and in disordered thin films,[27–29] Josephson junction arrays,[30] flux lines in dirty superconductors,[31] and alkali atoms in optical traps with disorder.[32–35] Superfluidity of liquid ^{4}He in a variety of porous media has been extensively investigated.[17] A goal is to determine the normal to superfluid transition temperature, T_C, and the critical exponents governing the superfluid density, $\rho_s(T)$, in confinement and disorder. T_c is suppressed below the bulk value, T_λ, by confinement and the critical exponents are larger or equal to the bulk values. Measurement of the excitations of liquid ^{4}He in porous media is relatively recent.[8,23,36–44] The aim is to determine how BEC and the phonon-roton (P-R) modes are modified by disorder and to make the connection with the changes in superfluid behavior.

The BEC condensate fraction in bulk liquid helium at low temperature is predicted to decrease significantly with increasing pressure,[4,45] from the observed value[40] of $n_0=7.25\%$ at saturated vapor pressure (SVP) ($p\simeq 0$) to $n_0\simeq 2\%-3\%$ at 40 bars. Thereafter n_0 decreases more slowly[4,45] and is predicted to remain finite at high pressure. This implies that bulk uniform liquid helium will remain a superfluid at higher pressure.[3] In contrast, in helium confined in 25 Å porous media, a quantum phase transition (QPT) from the superfluid to a normal liquid phase at $p_c=34$ bars at low temperature has been reported.[7,10] In this QPT the confinement and disorder in the porous media apparently play a critical role and the nature of the excitations and BEC in confined helium are of great interest.

Bulk liquid helium in equilibrium solidifies at 25.3 bars for temperatures $T\lesssim 1.0$ K. Werner *et al.*[1] extended the liquid phase of bulk helium from 25.3 up to 160 bars for short periods of time using rapid compression of the liquid. The liquid phase can also be extended to higher pressure when the liquid is confined in porous media.[5–8] In larger pore media (e.g., media with pore diameters $d\gtrsim 70$ Å), the increase in the freezing pressure, Δp, above the bulk value appears to be well predicted by the classical expression[2] $\Delta p=2\gamma/R$, where γ is the interface tension between the liquid and solid phases and $R=d/2$ is the radius of the pore. However, this expression for the onset of freezing pressure in a pore does not appear to hold well for small pore media ($d\lesssim 50$ Å). This is apparently because there is no well-defined surface between the liquid and solid phases during freezing at nanoscales.[46,47] The onset of freezing of ^{4}He in 25 Å mean pore diameter (mpd) gelsil has recently been measured[7] down to temperatures of $T=1.0$ K, where the onset of freezing pressure is at 38 bars. Extrapolation to temperatures be-

low 1.0 K suggests an onset of freezing at $p \simeq 36$ bars at $T \simeq 0$ K in 25 Å mpd gelsil.

In bulk superfluid helium, at pressures from SVP up 25.3 bars, the P-R mode is continuous and is sharply defined with a long lifetime[48–52] for wave vectors $0 \leq Q \leq 3.6$ Å. At a temperature of 1 K, the P-R mode lifetime is typically 1000 times longer than that of a longitudinal phonon in solid helium. Essentially, when there is BEC, the single-particle and density excitations in a Bose fluid[53–55] have the same energy. Thus there are no single-particle excitations at low energy to which the P-R mode can decay, as there is in liquid ^{3}He, for example. In a Bose condensed liquid, the P-R mode can decay only to other P-R modes, e.g., a single P-R mode into a pair of P-R modes. This later process has little phase space open to it and the mode has a long lifetime at low temperature. We expect this basic connection between BEC and the existence of only P-R modes to remain true at higher pressure.

The bulk modulus, the sound velocity and the P-R mode energy at lower wave vectors, Q, increase with pressure[8,48] and are predicted[4] to continue to increase with increasing pressure. In contrast, the P-R mode energy at higher wave vector in the roton region ($Q \simeq 2.1$ Å^{-1}) decreases with increasing pressure[8,48,56] and is predicted[4] to continue to decrease with increasing pressure. Thus the P-R mode energy dispersion curve spans a wider energy range at higher pressure with the energy of higher energy modes increasing in energy and the roton energy decreasing. This change opens up intermode decay channels. At $p \gtrsim 25$ bars the energy of the highest energy P-R modes at $Q \simeq 1.1$ Å^{-1} exceeds the energy of two rotons and the energy is high enough that the mode can decay into two rotons. Equivalently, we may say the high energy single P-R modes lie in the two P-R mode bands. These high energy modes broaden and become unobservable at $p \gtrsim 25$ bars.[8,56,57] As pressure is further increased, P-R modes over a wider range of Q around the "maxon" $Q \simeq 1.1$ Å^{-1} have sufficient energy to decay into two rotons and they too become broad and unobservable.[8,56,57]

In previous neutron-scattering measurements, we have observed the P-R modes of liquid ^{4}He at SVP ($p \simeq 0$) in several porous media.[38–40,44,58,59] Specifically the temperature dependence was investigated. This showed that well-defined P-R modes exist at temperatures above the superfluid phase of ^{4}He in the porous media, above T_c. Well-defined modes were generally observed up to or close to T_λ, the superfluid-normal transition temperature in bulk liquid helium ($T_\lambda = 2.17$ K at SVP), where T_λ is always greater than T_c. This was observed first in Vycor,[40,44] where $T_c = 2.05$ K, then in 25 Å mpd gelsil[56,58] ($T_c = 0.7$ to 1.3 K)[7,60] and in 44 Å mpd gelsil[59] ($T_c = 1.92$ K). Since well-defined P-R modes exist because there is BEC, this suggests that there is BEC above T_c in porous media. This was interpreted[23,24,40,44,58,59] as BEC localized to islands separated by normal liquid in the porous media, each island having an independent phase so that there was no phase coherence across the sample. This is a striking example of a Bose glass phase (at temperatures $T_c < T < T_\lambda$) which has been predicted to separate the superfluid and fully normal phase in dirty Bose systems.[18–22,61–64]

In this paper we present data on the P-R modes and other excitations of liquid helium in 25 and 34 Å mpd gelsil as function of pressure up to 54 bars and temperatures up to 2 K. Some data in 47 Å MCM-41 are also presented. We find that the P-R mode at wave vectors $Q \simeq 1.1$ Å^{-1} (the maxon region) broadens and becomes unobservable at the lowest pressures $p \gtrsim 26$ bars, as observed earlier[8] in a 44 Å mpd gelsil. At $p \simeq 26$ bars the single P-R mode energy ω_Q at $Q \simeq 1.1$ Å^{-1} exceeds twice the roton energy ($\omega_Q \geq 2\Delta$) and mode has sufficient energy to decay into two rotons. As pressure increases, the range of Q for which $\omega_Q \geq 2\Delta$ increases, around $Q \simeq 1.1$ Å^{-1}. At $p = 31.2$ bars we observe well-defined P-R modes at wave vectors $1.6 \leq Q \leq 2.3$ Å^{-1} only (where $\omega_Q \leq 2\Delta$). This mode decay process is an intrinsic property of liquid helium and we expect similar behavior in bulk liquid helium. We also expect the liquid to support long-wavelength phonons at $Q \lesssim 0.5$ Å (where again $\omega_Q \leq 2\Delta$) but apparently their intensity is too small to be observed in the present small pore media.

At $p = 36.3$–36.8 bars at low temperature, the P-R modes in the roton region also broaden and become unobservable in all the porous media investigated. There are no P-R modes at all above this pressure. We interpret this as the pressure at which either all BECs vanish in the liquid or there is significant solidification in the media. This pressure is above $p_c = 34$ bars, the pressure at which the QPT in 25 Å mpd gelsil is observed.[7,9] Similarly, at $p = 31.2$ bars, the P-R modes in the roton region broaden with increasing temperature and become unobservable at $T = 1.3$–1.4 K. At $p = 31.2$ bars, the T_c of the superfluid phase in 25 Å gelsil[7] is $T_c \simeq 0.2$ K. Thus there is a temperature range at 31.2 bars, $T_c \leq T \leq 1.4$ K, where there is BEC but no macroscopic superflow. We interpret this as the range where there is BEC localized to isolated islands that support P-R modes in an otherwise normal liquid, a Bose glass phase as in the range $T_c \leq T \leq T_\lambda$ at SVP.[23,24,40,44,58,59] A letter describing some of these results has appeared.[56]

The experiment is discussed below. The results are presented in Sec. III and the findings are discussed in Sec. IV.

II. EXPERIMENT

A. Porous media samples

Both the 25 and 34 Å mpd gelsils were fabricated by 4F International Co.[65] using a sol-gel technique. They were characterized by 4F International using N_2 adsorption-desorption isotherms at 76 K. The isotherms were analyzed using the standard Barrett, Joyner, and Halenda (BJH) model[66] revealing the mean pore diameters quoted with a broad approximately Gaussian pore diameter distribution of half width at half maximum of approximately 20 Å. The distribution of pore radii of the 34 Å mpd gelsil is shown in Fig. 1.

The 34 Å mpd sample had a pore volume of 0.539 cm^3/g and surface area of 638 m^2/g as determined from the isotherms using the Brunauer, Emmett, and Teller (BET) model[67] analysis. The 25 Å mpd sample had a pore volume of 0.376 cm^3/g and surface area of 586 m^2/g as determined similarly by 4F International Co. from the iso-

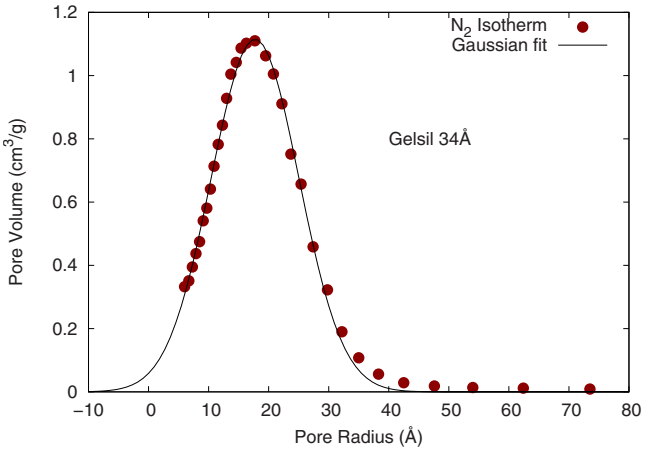

FIG. 1. (Color online) The distribution of pore radii in 34 Å mpd gelsil obtained from nitrogen isotherms by 4F International Co.

therms. The larger pore volume of the 34 Å gelsil meant that it held more helium and was a significantly easier sample to investigate with neutrons than the 25 Å mpd sample. The 25 Å mpd gelsil was kindly provided by Shirahama.[7,9,10] It is the same gelsil as used in his group's measurements of the superfluid density, the specific heat, and the phase diagram of helium in 25 Å gelsil.

The MCM-41 was synthesized by the group of Patarin and Soulard at the Laboratoire de Matériaux Minéraux, Mulhouse, France following the procedure of Corma *et al.*[68] The sample was a white powder of micrometer grain size. N_2 isotherms were performed and analyzed by them using the BJH model. This yielded a mean pore diameter of 47 Å with a narrow distribution around the mean of half width at half maximum of 1.5 Å, much narrower than the gelsil samples. A surface area of 931 m^2/g was determined using the BET procedure. The sample was the same as used previously by Albergamo *et al.*[43] to establish negative pressures and helium isotherms performed are reported in Ref. 43.

The samples were outgassed at 50 °C in a vacuum of 10^{-8} mbar for three days.

B. Neutron-scattering experiment

The gelsil samples consisted of two monolithic cylinders placed one on top of the other in the cylindrical Al sample cell as shown in Fig. 2. Specifically, the 34 Å mpd gelsil sample had a total mass of 2.58 g and volume 2.39 cm^3 in the form of two cylinders: one of diameter 9.2 mm and height 18.3 mm and the other of diameter 9.0 mm and height 18.5 mm. With a pore volume of 0.539 cm^3/g, a total sample pore volume of 1.39 cm^3 is indicated (a porosity of 58%). Similarly, the 25 Å mpd gelsil had a total mass of 2.93 g and volume 2.16 cm^3 in the form of two cylinders: one of diameter 8.76 mm and height 17.64 mm and the other of diameter 8.85 mm and height 17.79 mm. With a pore volume of 0.376 cm^3/g, a total sample pore volume of 1.11 cm^3 is indicated (a porosity of 51%).

The internal diameter of the sample cell is 10.2 mm for the 34 Å gelsil and 9.1 mm for the 25 Å gelsil. The volume

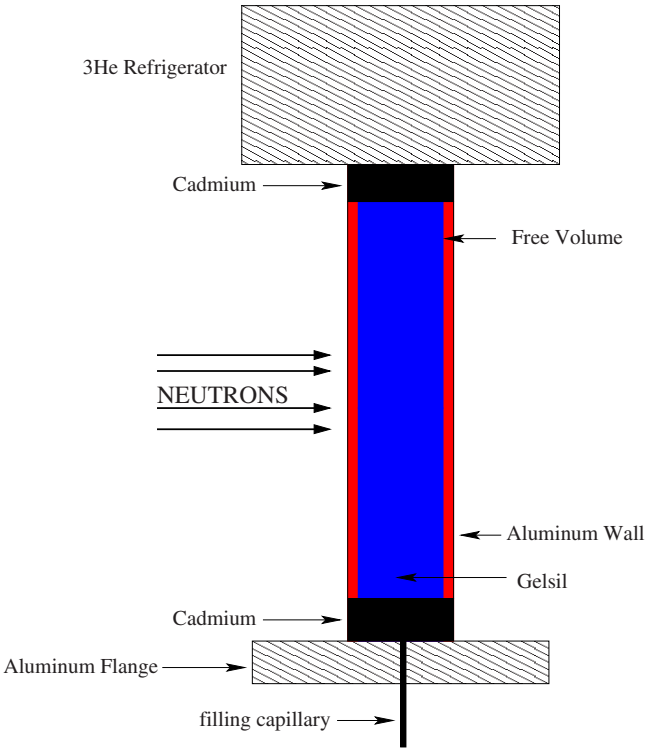

FIG. 2. (Color online) Schematic diagram of the gelsil sample and sample cell. The 34 Å gelsil contains $V=0.7$ cm^3 of liquid ^{4}He. There is $V=0.6$ cm^3 between the gelsil and the cell walls in the neutron beam. There is an additional $V=0.3$ cm^3 of liquid ^{4}He above and below the gelsil shielded from the neutron beam.

of helium between the gelsil and the cell walls exposed to the neutron beam (as shown in Fig. 2) is 0.61 cm^3 for the 34 Å gelsil and 0.15 cm^3 for the 25 Å gelsil. There is an additional volume of 0.3 cm^3 of helium above and below the sample shielded from the neutron beam by Cd rings in each case. The helium between the sample and the sample cell walls is bulk helium. This helium will exhibit bulk excitations and will solidify at 25.3 bars. In the case of the 47 Å mpd MCM-41, the sample in the form of a powder was packed gently in the cell. Although there is no bulk helium between the sample and the cell walls, there is bulk helium between the grains of the MCM-41 powder. The sample cell was cooled with a circulating ^{3}He cryostat for the 34 Å gelsil and the MCM-41 samples and by a dilution fridge for the 25 Å gelsil to reach lower temperatures.

The helium in the gelsil and MCM-41 pores consists of "dead" layers on the pore walls and liquid (or solid at high pressures). Approximately one half of the helium is in the dead layers in the 34 Å gelsil. The dead layers are expected to be layers of amorphous solid helium as discussed at the end of Sec. III and in Sec. IV B.

The porous media in the sample cell, shown in Fig. 2, were filled with helium via the filling capillary which is the warmest point in the sample cell. Particularly, at pressures above 25.3 bars the cell was filled at constant temperature and pressure with the filling capillary open. Above 25.3 bars the helium condenses as liquid in the gelsil and as bulk solid helium in the free space around the gelsil. The pressure was

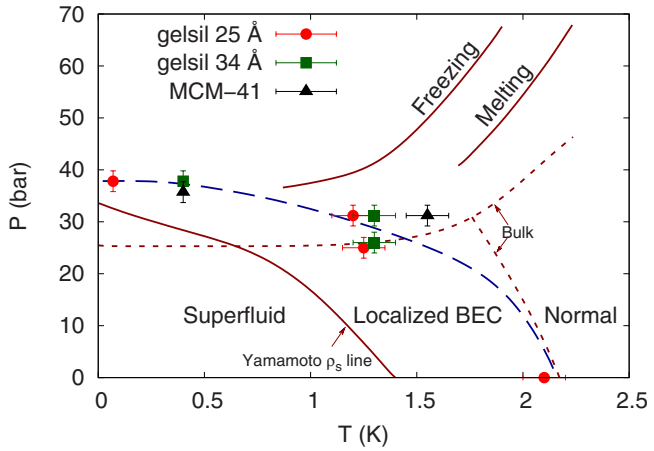

FIG. 3. (Color online) Phase diagram of P-R modes of ^{4}He in 25 and 34 Å mpd gelsil and 47 Å MCM-41. P-R modes are observed in the superfluid and localized BEC regions with the solid dots and long-dashed line showing the pressure and temperature at which well-defined P-R modes are last observed, marking the boundary of existence of BEC. At SVP ($p \simeq 0$), P-R modes are observed (Refs. 58 and 59) up to temperatures $T \simeq T_\lambda = 2.17$ K, at $p = 31.2$ bars up to $T \simeq 1.4$ K. The solid lines show the boundary of the superfluid phase (Ref. 7) and the onset of freezing and melting (Ref. 69) in 25 Å mpd gelsil. The short-dashed lines are the phase boundaries in bulk ^{4}He.

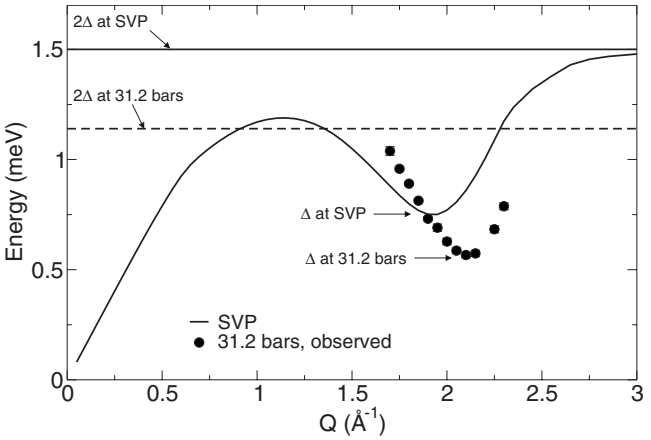

FIG. 4. The solid lines show the P-R energy, ω_Q, dispersion curve and twice the roton energy (2Δ) at SVP ($p \simeq 0$). The solid dots show the observed P-R dispersion curve at $p = 31.2$ bars and the dashed line the corresponding 2Δ. At $p = 31.2$ bars, P-R modes are observed at wave vectors in the range $1.6 \leq Q \leq 2.4$ Å^{-1} only where $\omega_Q \leq 2\Delta$.

determined from the temperature and the known pressure-temperature relations on the bulk melting line. When the cell is full, the capillary is blocked and the cell is isolated. When the cell is subsequently cooled below the bulk melting line, the pressure in the cell is calculated from the temperature. For example, for samples grown on the bulk melting line at $p = 37.8$ bars ($T = 2.00$ K), the pressure at the lowest temperature ($T = 0.07$ K) is calculated to be 36.3–36.8 bars. If the sample is grown at a pressure above 40 bars and there is solidification in the gelsil on cooling, the pressure in the cell is less accurately known at low temperature.

The inelastic neutron-scattering measurements were performed on the IN6 time-of-flight neutron spectrometer at the Institut Laue-Langevin (ILL), Grenoble, France. An incident neutron wavelength of 4.15 Å and spectrometer energy resolution full width at half maximum (FWHM) of 0.2 meV was used. The procedure for carrying out the neutron-scattering measurements was similar to that in previous experiments.[8,39,40,44,58,59] The data were analyzed using the standard ILL data analysis package LAMP available on the ILL website.

III. RESULTS

A. Modes: Pressure dependence

To set the stage for our experimental results we sketch the phase diagram of helium in Fig. 3. The short-dashed line marks the phase boundaries in bulk helium. At low temperature and low pressure, bulk helium is in the superfluid phase. At pressures above the short-dashed line, bulk helium solidifies, e.g., above 25.3 bars at $T \lesssim 1$ K. At higher temperature, the dashed line denotes the superfluid to normal liquid transition temperature T_λ. At SVP ($p \simeq 0$), $T_\lambda = 2.17$ K and on the bulk freezing line $T_\lambda = 1.76$ K. The solid line in Fig. 3 marks the phase boundaries of helium confined in 25 Å mpd gelsil.[10] At SVP, helium in the present 25 Å gelsil is a superfluid below $T_c = 1.4$ K. Clearly, T_c is suppressed below the bulk value T_λ by confinement. As pressure is increased, T_c decreases further until T_c goes to zero at a pressure $p = 34$ bars.[7] The superfluid-normal liquid (S-N) transition line (T_c) in 25 Å gelsil, where ρ_S is observed by Yamamoto *et al.*[7] to go to zero, is marked by a solid line. The solid lines labeled "freezing" and "melting" mark the onset of freezing and melting of helium in 25 Å gelsil as observed by Shirahama and co-workers[69,70] in pressure cell measurements. Clearly, in gelsil the liquid phase is extended up to higher pressures. Finally, the points with error bars denote the pressures and temperatures at which we last observe P-R modes in 25 and 34 Å mpd gelsil and in 47 Å MCM-41 in the present measurements as set out below. The existence of P-R modes signals the existence of liquid helium. It is also interpreted as signaling the existence of BEC in the liquid.[24,40,43,58,59]

Our measurements of the P-R modes as a function of pressure show that the P-R modes begin to broaden and disappear above 25.3 bars. The high energy modes in the maxon region broaden and become unobservable at the lowest pressure. To illustrate why high energy P-R modes broaden and disappear first, we show the P-R energy dispersion curve observed in bulk superfluid helium at SVP and in helium at 31.2 bars in 34 Å mpd gelsil in Fig. 4. At any wave vector Q, the energy of the sharp component of the phonon-roton response, which defines the P-R energy ω_Q, cannot exceed twice the roton energy 2Δ. If it does, the mode has sufficient energy to decay into two rotons. For example, at SVP, the energy of the P-R mode at higher Q beyond the roton comes up to 2Δ but does not exceed 2Δ.

As pressure increases, the roton energy decreases[8,48] (cf. Fig. 9). Also as pressure increases, the P-R mode energy, ω_Q,

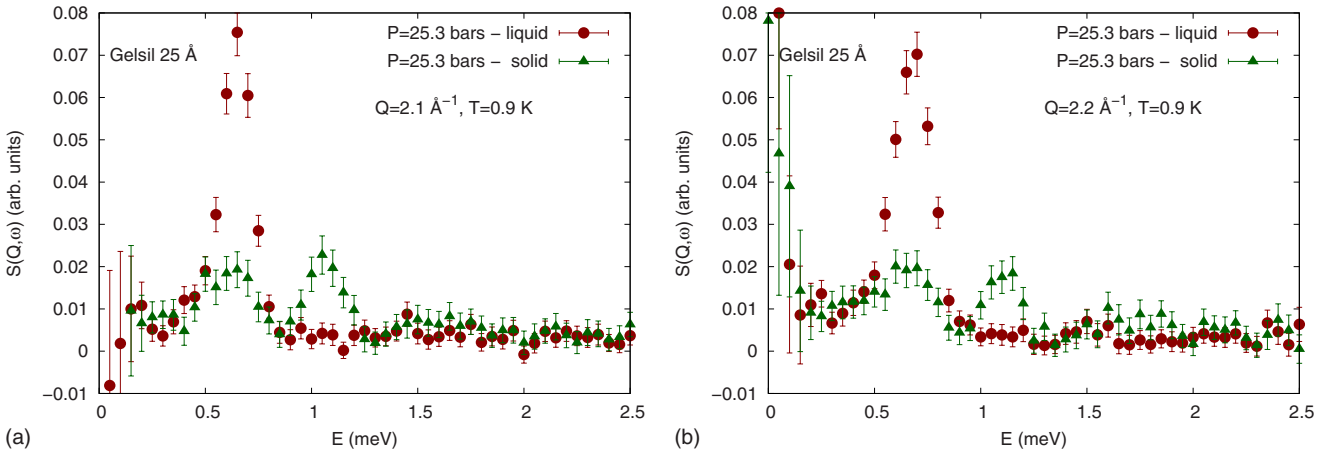

FIG. 5. (Color online) The dynamic structure factor $S(Q,\omega)$ of ^{4}He in 25 Å mpd gelsil at $Q=2.1$ and 2.2 Å^{-1} and $T=0.9$ K at pressures (1) $p \lesssim 25.3$ bars with liquid in and liquid around the gelsil (liquid) and (2) $p \gtrsim 25.3$ bars with liquid in the gelsil and solid around the gelsil (solid). The intensity in the P-R mode ($\omega \simeq 0.62$ meV) arising from liquid in the gelsil only (when $p \geq 25.3$ bars) is much weaker than that from the bulk liquid around the gelsil when $p \lesssim 25.3$ bars. The intensity centered at $\omega \simeq 1.1$ meV observed when $p \gtrsim 25.3$ bars arises from phonons in the solid around the gelsil.

at wave vectors in the maxon region increases. At approximately 20 bars, ω_Q in the maxon region reaches 2Δ and ω_Q ceases to increase with increasing pressure. Above 25.4 bars, we no longer observe P-R modes in the maxon region because the mode has broadened through decay to two rotons. Indeed, at $p=31.2$ bars, as shown in Fig. 4, we observe modes at wave vectors in the range $1.6 < Q < 2.4$ Å^{-1} only where ω_Q lies below 2Δ. We can observe modes up to $Q=2.3$ Å^{-1} on the present neutron spectrometer only. Loss of P-R modes at Q values $0.6 < Q < 1.6$ Å^{-1} at $p=31.2$ bars can thus be understood in terms of mode decay to two modes because $\omega_Q \geq 2\Delta$. At Q values below 0.6 Å^{-1} the scattering intensity is low and this is probably why we do not observe phonons at $Q < 0.6$ Å^{-1} in the present small samples. We now focus on the remaining modes at wave vectors $1.6 < Q < 2.4$ Å^{-1}.

In Fig. 5 we show the dynamic structure factor $S(Q,\omega)$ at $Q=2.1$ and 2.2 Å^{-1} for $T=0.9$ K and pressures immediately below and above 25.3 bars where bulk helium freezes. Below 25.3 bars there is bulk liquid in the gelsil and around the gelsil. Below 25.3 bars, the roton mode in $S(Q,\omega)$ arises from both the liquid in the gelsil and around the gelsil and there is an intense P-R mode (roton) at $\omega \simeq 0.6$ meV. Immediately above 25.3 bars, the bulk liquid around the gelsil freezes and the intensity of the P-R mode in $S(Q,\omega)$ drops markedly on the scale shown. The remaining P-R mode arising from the superfluid in the gelsil at $p \geq 25.3$ bars has a clear width. Immediately above 25.3 bars we observe a peak at $\omega \simeq 1.1$ meV arising from exciting phonons in the solid around the gelsil. The purpose of Fig. 5 is to show that at higher pressure the peak intensity of the P-R modes in the gelsil is low and the mode has a width. In contrast, at SVP the scattering intensity from the P-R modes of superfluid ^{4}He in 44 Å^{-1} gelsil and in the bulk are comparable[59] and the modes have an unobservably small width.[39,58,59]

Figure 6 shows a color plot of the intensity in $S(Q,\omega)$ as a function of wave vector Q and energy ω transfer of ^{4}He at 25.4 bars in 25 Å mpd gelsil. The intensity of the P-R mode in $S(Q,\omega)$ is highest at the roton wave vector $Q=2.1$ Å (at energy $\omega \simeq 0.62$ meV). The intensity in the P-R mode decreases with decreasing Q until at $Q \leq 1.3$ Å^{-1} there is no observable P-R mode in the plot. There are some indications of increased intensity again in the P-R mode at $Q \simeq 0.8-0.9$ Å^{-1} in the phonon region. There is also large intensity at $Q \simeq 2.0$ Å and energy $\omega \simeq 1.0$ meV arising from phonons in the solid around the gelsil. The scattering intensity from single phonons (Q^2 times the Debye-Waller factor) in solid helium at this pressure is expected[49] to peak at 1.8–2.0 Å^{-1} consistent with the phonon intensity observed in Fig. 6.

The same features in $S(Q,\omega)$ are displayed in Fig. 7. At $Q=2.1$ Å^{-1} the P-R mode has large intensity peaked at ω

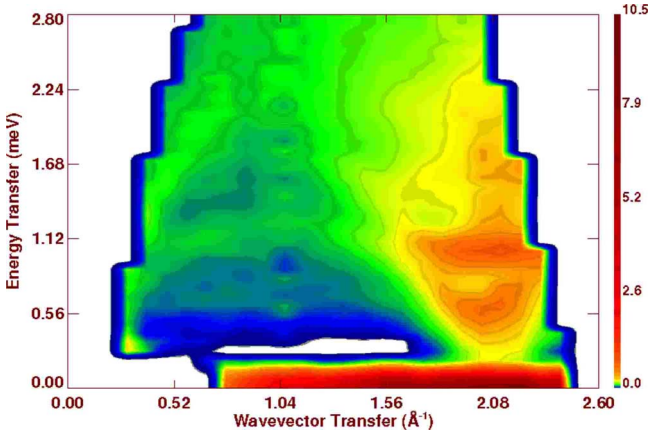

FIG. 6. (Color online) Intensity plot of $S(Q,\omega)$ in wave vector Q and energy ω of ^{4}He in 34 Å mpd gelsil at pressure $p=25.4$ bars. The intensity in the P-R mode in the roton region at $Q \simeq 2.1$ Å^{-1} and $\omega=0.62$ meV is high. The intensity in the P-R mode falls with decreasing Q until in the maxon region $Q \simeq 0.9-1.2$ Å, where the mode energy would be $\omega \simeq 2\Delta = 1.2$ meV; there is no peak intensity. There is some indication of a P-R mode in the phonon region at $Q \simeq 0.6-0.7$ Å. The intensity at higher energy arises from phonons in the solid around the gelsil.

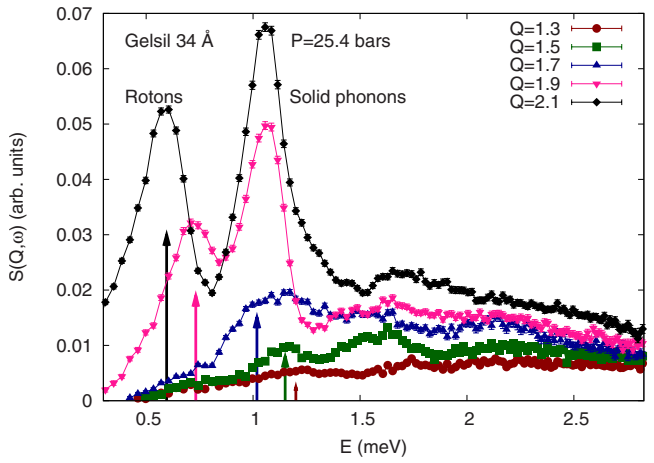

FIG. 7. (Color online) $S(Q,\omega)$ of ^{4}He in 34 Å^{-1} mpd gelsil at pressure $p=25.4$ bars at wave vectors $Q=1.3-2.1$ Å^{-1}. The arrows indicate the peak position in energy of the P-R mode. The intensity of the P-R mode in the roton region at $Q\simeq 2.1$ Å^{-1} and low energy $\omega\simeq 0.6$ meV is high. The intensity in the P-R mode falls with decreasing Q (increasing energy E) until at $Q=1.3$ Å and energy $\omega\simeq 1.2$ meV there is no well-defined peak. The large intensity at energy $\omega\simeq 1.1$ meV arises from phonons in the solid around the gelsil.

$\simeq 0.62$ meV. As Q is decreased toward the maxon region, the intensity in the P-R mode decreases (and the energy increases) until at $Q=1.3$ Å^{-1} only a very broad mode remains at $\omega\simeq 1.2$ meV or no mode at all. In the wave vector range $1.6<Q<2.4$ Å^{-1} (not shown) no P-R mode is observed. Again, large intensity arising from phonons in the solid around the gelsil is observed at $\omega\simeq 1.0$ meV at wave vectors $Q=1.7-2.1$ Å^{-1}.

Figure 8 shows the pressure dependence of $S(Q,\omega)$ at wave vectors $Q=2.1-2.3$ Å^{-1} in 25 Å mpd gelsil at low temperature. The inelastic response from the P-R mode is again peaked at $\omega\simeq 0.6$ meV and that from the phonons in the solid around the gelsil at $\omega\simeq 1.1$ meV. As pressure increases above 34 bars, the intensity in the P-R mode begins to decrease (or the mode broadens) and at a pressure of 37.8 bars a well-defined mode is no longer observed. Two separate samples were grown at $p=37.8$ bars in the 25 Å mpd gelsil. In one case a P-R mode was observed but not in the other. The difference probably arises from a small difference in the actual pressure. The pressure $p=37.8$ bars is the pressure at which the helium samples were grown at $T=2.0$ K. This corresponds to a pressure of 36.3–36.8 bars at $T=0.07$ K. A P-R mode has not been observed at a pressure above 36.3–36.8 bars in the 25, 34, and 44 Å mpd gelsils or 47 Å MCM-41 in our measurements. In Fig. 9 we plot the P-R mode energy at the roton wave vector versus pressure

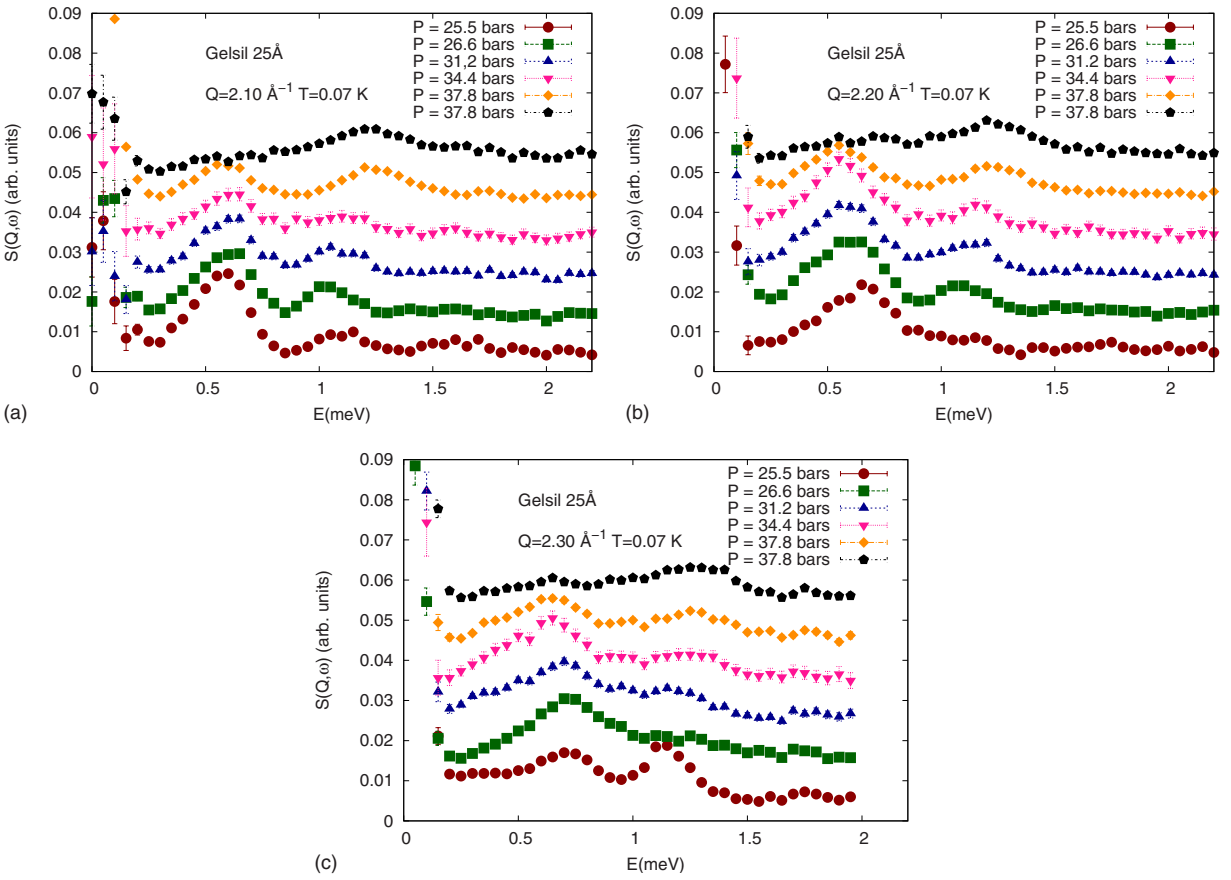

FIG. 8. (Color online) $S(Q,\omega)$ of ^{4}He at $Q=2.1-2.3$ Å^{-1} in 25 Å mpd gelsil as a function of pressure. In all cases, the P-R mode at $\omega\simeq 0.65$ meV is no longer observed at pressures $p=37.8$ bars and above. The pressure 37.8 bars is the pressure at which the cell was filled at $T=2.00$ K and blocked. The pressure at low temperature (e.g., $T=0.07$ K) is estimated to be $p=36.3-36.8$ bars. The peak at $\omega\simeq 1.1$ meV arises from phonons in the bulk solid ^{4}He that lies between the gelsil sample and the cell wall.

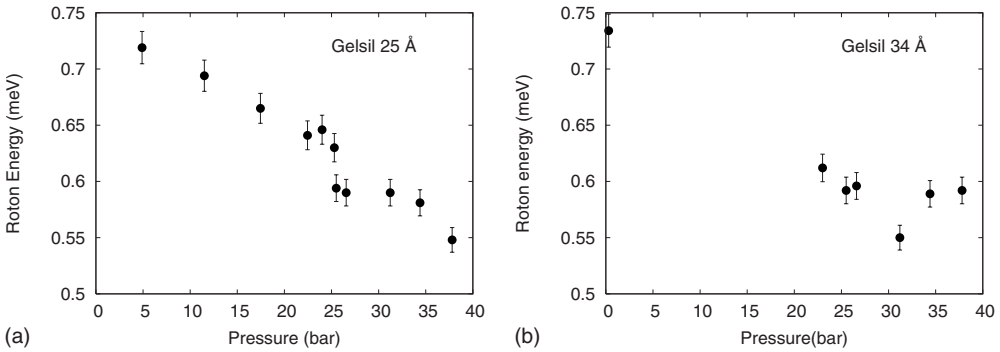

FIG. 9. The roton energy Δ versus pressure in 25 and 34 Å mpd gelsil. In 34 Å gelsil the roton energy appears to change little or erratically with pressure for $p \gtrsim 30$ bars which is not understood.

with no rotons observed in samples grown at pressures above 37.8 bars.

B. Modes: Temperature dependence

At higher pressures, $p=26$ and 31.2 bars, we find that well-defined P-R modes in liquid helium in the gelsils are observed up to $T=1.3-1.4$ K only. Figure 10 shows $S(Q,\omega)$ at the roton wave vector $Q=2.1$ Å^{-1} in 25 and 34 Å mpd gelsil as a function of temperature at $p=31.2$ bars. The large intensity at zero energy transfer ($\omega=0$) is elastic scattering from the gelsil and sample cell. The peak at 0.6 meV is the roton mode. The peak at $\omega \simeq 1.1$ meV again arises from phonons in the solid around the gelsil. As temperature is increased, the roton mode broadens and the intensity in the mode decreases. Some of this intensity are transferred to low ω. At $T=1.3-1.4$ K, there is no longer a well-defined roton mode in either gelsil. This is consistent with our previous findings[8] in 44 Å mpd gelsil. The temperature $T=1.3-1.4$ K at which the P-R modes are last observed at $p=31.2$ bar and $p=26$ bar is marked in the phase diagram in Fig. 3.

Figure 11 shows the temperature dependence of $S(Q,\omega)$ at the roton Q and $p=26$ bars where we see that there is no roton above $T=1.3-1.4$ K. $S(Q,\omega)$ at 70 bars is also shown. At 70 bars all the helium is expected to be solid and there is no scattering at low ω and the phonons have moved to higher energy as expected for phonons in the solid.

C. Structure factor

To investigate the freezing of the liquid and the structure of the solid in the pores of 34 Å mpd gelsil, we measured the static structure factor $S(Q)$ as a function of pressure. A background measurement was first made with helium at 5 K and SVP in the cell. In this background we expect to have amorphous solid helium layers on the pore walls but otherwise helium gas at SVP in the cell. Shown on the left side of Fig. 12 is the net $S(Q)$ above this background arising from ^{4}He at $T=0.4$ K in the gelsil pores and between the gelsil and the sample cell walls. At $p=25.4$ bars we anticipate liquid in the interior of the gelsil and bulk crystalline solid around gelsil. At $p=25.4$ bars the $S(Q)$ in Fig. 12 shows the structure expected for a liquid (or an amorphous solid) in the pores with a peak position at $Q \simeq 2.25$ Å^{-1}. There are also Bragg peaks which arise from the bulk crystalline solid around the gelsil. As pressure is increased up to 34.4 bars the peak position of $S(Q)$ moves to higher Q as expected for a

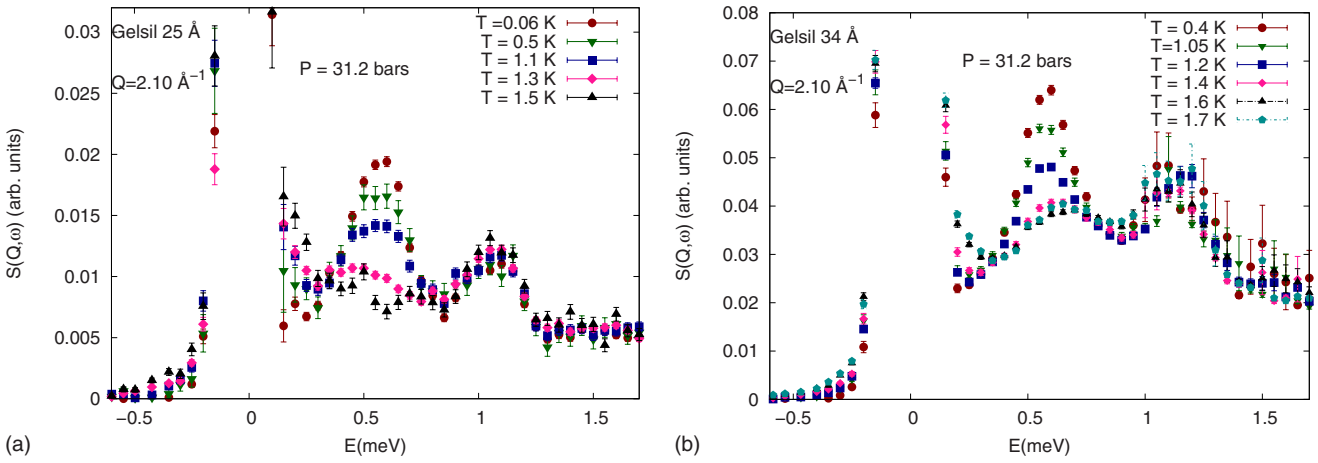

FIG. 10. (Color online) The temperature dependence of $S(Q,\omega)$ of ^{4}He in 25 and 34 Å mpd gelsil at $Q=2.1$ Å^{-1} and $p=31.2$ bars. The height of the roton mode peak at $\omega \simeq 0.6$ meV decreases with increasing temperature until a well-defined mode is no longer observed at $T \geq 1.4$ K. The peak at $\omega \simeq 1.1$ meV arises from phonons in the bulk solid ^{4}He that lies between the gelsil sample and the cell wall.

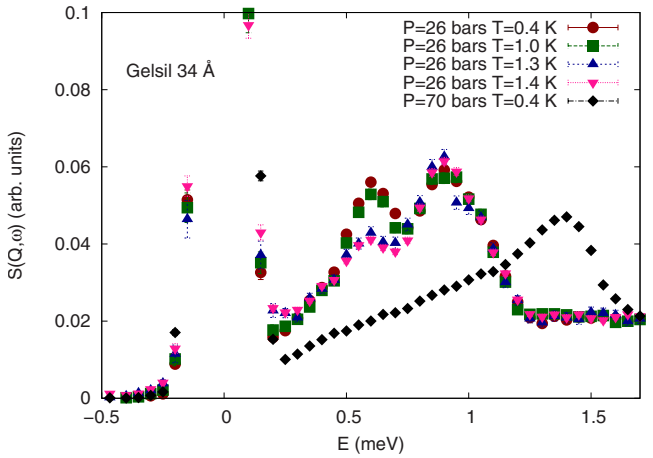

FIG. 11. (Color online) $S(Q,\omega)$ at $Q=2.1$ Å^{-1} and several temperatures chiefly at $p=26$ bars. At low temperature and 70 bars there is apparently no scattering intensity characteristic of a liquid. Between $p=26$ and 70 bars, the peak arising from phonons in the solid around the gelsil increases from $\omega\simeq 0.9$ meV to $\omega\simeq 1.4$ meV

liquid under increasing pressure. However, between 34.4 and 44.8 bars the peak position dropped to lower Q, as highlighted on the right side of Fig. 12. We associate the drop in peak position of $S(Q)$ between 34.4 and 44.8 bars with freezing of the liquid in the pores. The freezing is predominantly to an amorphous solid since the shape and intensity in $S(Q)$ has changed little from the liquid $S(Q)$.

There is possibly a broad Bragg peak appearing on solidification just below the main peak of $S(Q)$ which lowers the apparent peak position of $S(Q)$ as was observed in helium in a 70 Å mpd gelsil.[71] However, simulations of freezing in liquids of nanoscale size[47] suggest that solidlike correlations develop as freezing proceeds and these solidlike correlations lower the peak position of $S(Q)$ as observed in Fig. 12.

We have also observed Bragg peaks arising from the solid in the gelsil in some samples so that some crystalline regions in the gelsil are indicated. A fresh sample is grown at each pressure so that the Bragg peaks appear at different positions at different pressures. However, the $S(Q)$ is characteristic of an amorphous solid occupying most of volume in the 34 Å gelsil pores because the magnitude of $S(Q)$ differs little from that of the liquid. Thus only a small fraction of the intensity lies in Bragg peaks. Freezing and the solid phase are discussed further below and in a forthcoming publication.

D. Bulk solid phonons

We have interpreted the scattered intensity, shown in Figs. 6–8, 10, and 11, observed at higher energies (e.g., at $\omega\gtrsim 1$ meV for $Q\simeq 2.0$ Å^{-1}) as arising from phonons in the bulk solid helium lying between the gelsil and the sample cell walls. For example, in Fig. 6 the maximum in $S(Q,\omega)$ at $Q=2.1$ Å^{-1} and $\omega\simeq 1$ meV is attributed to phonons in bulk solid helium. This maximum lies immediately above the maximum in $S(Q,\omega)$ at $\omega\simeq 0.62$ meV arising from rotons.

To support this interpretation, we note first that the one phonon $S(Q,\omega)$ as a function of Q peaks at $Q\simeq 2$ Å^{-1} for phonons in solid hcp at $p\simeq 26$ bars ($V=21.1$ cm^3/mole, lattice constant $a=3.67$ Å) (see Fig. 4.3 of Ref. 49). Also, the phonon energy at this Q value in hcp solid helium at $a=3.68$ Å has recently been observed[72] to be 0.9–1.0 meV. Thus the position of the maximum of $S(Q,\omega)$ in Q and ω seen in Fig. 6 is exactly as expected for phonons in bulk hcp solid helium. It is curious that $S(Q,\omega)$ of hcp solid averaged over randomly oriented crystallites looks so similar to that of liquid helium when observed using a time-of-flight instrument with a resolution of 0.2 meV. The solid shows an "apparent" rotonlike minimum. However, the branches and orientation dependence expected for phonons in a solid (as well as observable phonon widths) are revealed in triple axis measurements.[73] Higher resolution would reveal that P-R modes in the liquid have orders of magnitude narrower line widths at $T\leq 1.0$ K.

Second, the phonon energies observed at $Q\simeq 2.1$ Å^{-1} and $\omega\simeq 1.1$ meV increase with increasing pressure, characteristic of phonons in a solid. This is seen particularly in Figs. 8

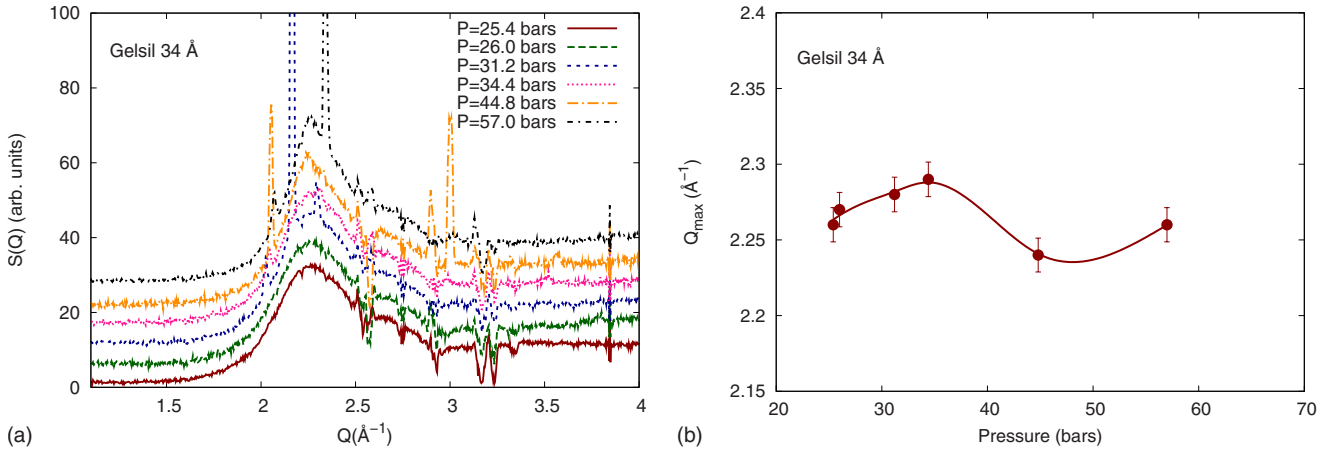

FIG. 12. (Color online) Left: $S(Q)$ of ^{4}He at $T=0.4$ K in and around 34 Å mpd gelsil. Right: Peak position of $S(Q)$ versus pressure. The peak position of $S(Q)$ moves to higher Q with increasing pressure up to 34 bars characteristic of a liquid under increasing pressure (Ref. 4) Between 34 and 45 bars the peak position decreases with increasing pressure signaling some freezing of the liquid to an amorphous solid in the gelsil. Bragg peaks are also observed arising from crystalline solid around the gelsil. A fresh sample is grown at each pressure.

and 11. In contrast the roton energy decreases with increasing pressure. As Q is reduced toward 1.3 Å^{-1}, the scattering intensity from both the phonon-roton mode in the liquid and from the phonons in the solid becomes weak and broad. At these Q values it is difficult to separate the two unambiguously.

Third, there is a larger volume of solid helium around the 34 Å gelsil than around the 25 Å gelsil. The observed scattering intensity at $\omega \simeq 1.1$ meV is larger for the 34 Å gelsil (see Fig. 7) than observed for the 25 Å gelsil in Fig. 8. This is consistent with the intensity at $\omega \simeq 1.1$ meV arising from phonons in the solid. The intensity arising from the solid phonons relative the roton intensity varies from pressure to pressure since a new solid is grown at each pressure (new solid orientations).

IV. DISCUSSION AND INTERPRETATION

A. Quantum phase transition and the Bose glass phase

As discussed in Sec. III and shown in Figs. 3 and 8, we observe P-R modes at wave vectors in the roton region in 25 and 34 Å mpd gelsil up to but not beyond a pressure $p_B = 36.3-36.8$ bars at $T \leq 0.5$ K. This pressure exceeds the pressure $p_c = 34$ bars at which Yamamoto *et al.*[7] observe the superfluid density ρ_S to go to zero in 25 Å gelsil. Since there is roton up to p_B, there must be liquid up to p_B, at least in domains large enough to support a roton mode. (The number of atoms in a 25 Å pore excluding the amorphous solid "dead" layer on the walls is approximately 100.) At the same time, the onset of freezing line observed by Shirahama *et al.*[10,69] and shown in Fig. 3 extrapolates to between 34.5 and 36.5 bars at low temperature. Thus p_B lies close to or even somewhat above the onset of some solidification in the 25 gelsil. However, as discussed below, the onset of freezing probably represents freezing of only a small fraction of the liquid. With this introductory sketch we make the following comments on the results of Sec. III.

(1) The observation of a P-R mode at p_B means that in the pressure range $p_c < p < p_B$ the helium is predominantly liquid. The observation of P-R modes at pressures above p_c supports the interpretation that p_c is the critical pressure of a QPT from a superfluid to a Bose glass within the liquid rather than the ρ_S going to zero at p_c because of solid formation.

(2) Since well-defined P-R modes require BEC, this means that there must be BEC up to the pressure p_B. Thus the pressure range $p_c < p < p_B$ represents a pressure range in which there is localized BEC in the liquid in the same way that there is localized BEC in the temperature range $T_c < T < T_\lambda$ at SVP. At a pressure of 35 bars, the condensate fraction in bulk liquid helium is predicted[4,45] to be 2%–4%. For helium in cylindrical pores, Rossi *et al.*[75] predicted a condensate fraction that varies from layer to layer of helium within the pore with an average fraction of 1% at 68 bars.

(3) From the phase diagram in Fig. 3, we see that there is localized BEC surrounding the superfluid phase in the 25 Å gelsil at all the pressures and temperatures investigated. This suggests that there is indeed a Bose glass phase separating the superfluid and normal liquid phases at all pressures and temperatures.

(4) With localized BEC surrounding the superfluid, the superfluid to normal liquid phase transition may be interpreted as an extended to localized BEC crossover. In the superfluid phase, the condensate is extended and continuous with a single phase across the sample. There is phase coherence across the sample. Above T_c, or above p_c at $T \simeq 0$ K, the condensate is sufficiently localized to islands separated by normal fluid that there is no phase coherence across the sample.

(5) At the lowest temperatures, the P-R mode could disappear because of loss of BEC in the liquid or because of sufficient solidification of the liquid in the gelsil to eliminate the P-R modes. At higher temperatures, however, the P-R mode definitely disappears in the liquid phase. For example, at $T = 1.3-1.4$ K, the P-R mode is last seen at pressures (e.g., 31.2 bars) that lie well below the freezing line[7,9] reproduced in Fig. 3. In this case, we may associate the loss of P-R modes with the loss of localized BEC in the liquid phase. The loss of P-R modes in the liquid under pressure at higher temperature is confirmed in recent specific-heat measurements.[10]

B. Freezing of the liquid

The classical expression for the increase in freezing pressure, Δp, in a pore of diameter d above the bulk liquid freezing pressure is $\Delta p = 4\gamma/d$, where γ is the interface tension between the solid and liquid phases. In a porous media having a broad distribution of pore diameters such as the gelsils, the classical expression suggests a distribution of freezing pressures in the media. This expression predicts a mean freezing pressure of 65 bars in the 34 Å mpd gelsil using the pressure-dependent γ proposed by Maris and Caupin.[2] It suggests a distribution of freezing pressures of FWHM of $\delta p = \Delta p(\delta d/d) \simeq \Delta p \simeq 40$ bars with an onset of freezing at the edge of the FWHM of 40–45 bars. If there is a dead layer on the media walls, the pore diameter d should be reduced by the width of the dead layers.

While valid for large pore media,[2] we expect this classical result to be at best an indicator for smaller pore media such as the present gelsils. Indeed, Bittner and Adams[5] found the freezing pressure independent of pore diameter in smaller pore media. First, the classical expression is obtained by assuming that there is solidification to a well-defined solid phase (e.g., crystalline) so that there is a meaningful surface tension between the solid and the liquid phases. It is also assumed that the solid regions nucleate in the liquid away from the walls and that solidification proceeds by growth of these regions once they reach a critical size. However, simulations of freezing in small pores of diameter $d \leq 20\sigma$, where σ is the diameter of a hard sphere representing the helium atom ($\sigma \simeq 2.203$ Å for helium[74]) indicate that the liquid freezes to an amorphous solid which is difficult to distinguish from the liquid.[46,47] Rather than having a well-defined solid and liquid phases, solidlike correlations develop within the liquid as freezing proceeds to an amorphous solid. Simulations suggest that the static structure factor, $S(Q)$, of the

amorphous solid regions differs little from that of the liquid. Indeed, the only difference in $S(Q)$ on solidification is an increase in the peak height of the main peak in $S(Q)$ on the low Q side of the peak,[47] exactly as we observe in Fig. 12. In larger 70 Å mean pore diameter gelsil, Wallacher *et al.*[71] observed a single broadened Bragg peak on freezing. We have observed Bragg peaks in some samples of freezing in the present 25–44 Å mpd gelsils but usually Bragg peaks are not observed.

Specifically, simulations of argon in small pore disordered carbon[47] find that freezing begins with a few regions of the liquid developing interatomic correlations characteristic of an amorphous solid. The number of regions showing amorphous solid correlations grows as the temperature is lowered. As temperature is further decreased the "solidified" regions coalesce giving way to larger connected regions of amorphous solid. The density increases gradually as the total fraction of the liquid showing amorphous solid correlations increases.

Rossi *et al.*[75] find that freezing of helium confined in a 25 Å diameter cylinder takes place layer by layer. In the liquid phase at low pressure, there is always a "dead" layer of ^{4}He adsorbed on the cylinder walls which is an amorphous solid, as observed on aerogel,[76] for example, and as we observe in the present gelsils. The first layer beyond the "dead" layer is liquidlike as are subsequent layers at low pressure. As pressure is increased, the first liquid layer adjacent to the wall freezes with subsequent internal layers freezing at higher pressure.[75] The freezing takes place layer by layer to an amorphous structure in each layer over a range of pressures.

In all the above pictures we expect freezing in the gelsils over a range of pressures. At higher pressure a larger fraction of the liquid freezes since subsequent liquid layers freeze. The simple picture of layer by layer freezing is complicated by the irregular nature of the gelsils and the broad distribution of pore diameters. In the 25 Å mpd gelsils, Shirahama[69] observed onset of freezing at 38.9 bars at $T=1.2$ K with a small pressure drop on freezing of $\delta p \simeq 0.6$ bars. Freezing at higher pressures $p=41.5$ bars and $p=49.0$ bars shows a larger pressure drop on freezing, $\delta p \simeq 1.7$ bars and $\delta p \simeq 3.0$ bars, respectively. The larger pressure drop suggests that a larger fraction of the liquid is solidifying at higher pressures. This is consistent with layer by layer freezing and with growing regions developing solidlike interatomic correlations as pressure increases. It is also consistent with our measurements of $S(Q)$ which show freezing to an amorphous solid that is structurally little different from the liquid even up to 57 bars.

Parenthetically, it is interesting that simulations predict liquid regions up to high pressures (62 bars in 70 Å Vycor[77] and 200 bars in 25 Å gelsil[46]) but these regions are apparently not superfluid as indicated by the small superfluid density in solid helium in Vycor. We plan to return to this topic in a future publication.

ACKNOWLEDGMENTS

The authors thank K. Shirahama for supplying the 25 Å mpd gelsil sample and for valuable discussions. Support from the Institut Laue Langevin is greatly appreciated. This work was partially supported by U.S. DOE under Grant No. DOE-FG02-03ER46038.

*Present address: National Physical Laboratory, Hampton Road, Teddington TW11 0LW, United Kingdom.

[1] F. Werner, G. Beaume, A. Hobeika, S. Nascimbène, C. Herrmann, F. Caupin, and S. Balibar, J. Low Temp. Phys. **136**, 93 (2004).
[2] H. Maris and F. Caupin, J. Low Temp. Phys. **131**, 145 (2003).
[3] P. Nozières, J. Low Temp. Phys. **142**, 91 (2006).
[4] L. Vranješ, J. Boronat, J. Casulleras, and C. Cazorla, Phys. Rev. Lett. **95**, 145302 (2005).
[5] D. N. Bittner and E. D. Adams, J. Low Temp. Phys. **97**, 519 (1994).
[6] E. B. Molz and J. R. Beamish, J. Low Temp. Phys. **101**, 1055 (1995).
[7] H. Yamamoto, H. Nakashima, Y. Shibayama, and K. Shirahama, Phys. Rev. Lett. **93**, 075302 (2004).
[8] J. V. Pearce, J. Bossy, H. Schober, H. R. Glyde, D. R. Daughton, and N. Mulders, Phys. Rev. Lett. **93**, 145303 (2004).
[9] K. Yamamoto, Y. Shibayama, and K. Shirahama, J. Phys. Soc. Jpn. **77**, 013601 (2008).
[10] K. Shirahama, K. Yamamoto, and Y. Shibayama, Low Temp. Phys. **34**, 273 (2008).
[11] K. Yamamoto, Y. Shibayama, and K. Shirahama, Phys. Rev. Lett. **100**, 195301 (2008).
[12] E. Kim and M. Chan, Science **305**, 1941 (2004).
[13] E. Kim and M. Chan, Nature (London) **427**, 225 (2004).
[14] Ann Sophie C. Rittner and J. D. Reppy, Phys. Rev. Lett. **98**, 175302 (2007).
[15] S. Sasaki, R. Ishiguro, F. Caupin, H. J. Maris, and S. Balibar, Science **313**, 1098 (2006).
[16] J. Day and J. R. Beamish, Nature (London) **450**, 853 (2007).
[17] J. D. Reppy, J. Low Temp. Phys. **87**, 205 (1992).
[18] M. P. A. Fisher, P. B. Weichman, G. Grinstein, and D. S. Fisher, Phys. Rev. B **40**, 546 (1989).
[19] K. Huang, in *Bose Einstein Condensation*, edited by A. Griffin, D. Snoke, and S. Stringari (Cambridge University Press, Cambridge, 1995), p. 31.
[20] M. Ma, P. Nisamaneephong, and L. Zhang, J. Low Temp. Phys. **93**, 957 (1993).
[21] G. E. Astrakharchik, J. Boronat, J. Casulleras, and S. Giorgini, Phys. Rev. A **66**, 023603 (2002).
[22] A. V. Lopatin and V. M. Vinokur, Phys. Rev. Lett. **88**, 235503 (2002).
[23] H. R. Glyde, F. Albergamo, R. T. Azuah, J. Bossy, and B. Fåk, Eur. Phys. J. E **12**, 63 (2003).
[24] H. R. Glyde, Eur. Phys. J. Spec. Top. **141**, 75 (2007).
[25] E. W. Carlson, V. J. Emery, S. A. Kivelson, and D. Orgad, in *The*

Physics of Conventional and Unconventional Superconductors, edited by K. H. Bennemann and J. B. Ketterson (Springer-Verlag, Berlin, 2002).
[26] N. Trivedi, A. Ghosal, and M. Randeria, Int. J. Mod. Phys. B **15**, 1347 (2001).
[27] N. Marković, C. Christiansen, A. M. Mack, W. H. Huber, and A. M. Goldman, Phys. Rev. B **60**, 4320 (1999).
[28] A. M. Goldman, Physica E (Amsterdam) **18**, 1 (2003).
[29] K. A. Parendo, K. H. Sarwa B. Tan, and A. M. Goldman, Phys. Rev. B **73**, 174527 (2006).
[30] A. van Otterlo, K. H. Wagenblast, R. Fazio, and G. Schon, Phys. Rev. B **48**, 3316 (1993).
[31] U. C. Tauber and D. R. Nelson, Phys. Rep. **289**, 157 (1997).
[32] Y. Kawaguchi, H. Saito, and M. Ueda, Phys. Rev. Lett. **97**, 130404 (2006).
[33] C. Fort, L. Fallani, V. Guarrera, J. E. Lye, M. Modugno, D. S. Wiersma, and M. Inguscio, Phys. Rev. Lett. **95**, 170410 (2005).
[34] J. E. Lye, L. Fallani, M. Modugno, D. S. Wiersma, C. Fort, and M. Inguscio, Phys. Rev. Lett. **95**, 070401 (2005).
[35] D. Clement, A. F. Varon, M. Hugbart, J. A. Retter, P. Bouyer, L. Sanchez-Palencia, D. M. Gangardt, G. V. Shlyapnikov, and A. Aspect, Phys. Rev. Lett. **95**, 170409 (2005).
[36] G. Coddens, J. de Kinder, and R. Millet, J. Non-Cryst. Solids **188**, 41 (1995).
[37] R. M. Dimeo, P. E. Sokol, C. R. Anderson, W. G. Stirling, K. H. Andersen, and M. A. Adams, Phys. Rev. Lett. **81**, 5860 (1998).
[38] O. Plantevin, B. Fåk, H. R. Glyde, J. Bossy, and J. R. Beamish, Phys. Rev. B **57**, 10775 (1998).
[39] B. Fåk, O. Plantevin, H. R. Glyde, and N. Mulders, Phys. Rev. Lett. **85**, 3886 (2000).
[40] H. R. Glyde, O. Plantevin, B. Fåk, G. Coddens, P. S. Danielson, and H. Schober, Phys. Rev. Lett. **84**, 2646 (2000).
[41] B. Fåk and H. R. Glyde, in *Advances in Quantum Many-Body Theory*, edited by E. Krotscheck and J. Navarro (World Scientific, Singapore, 2002), Vol. 4.
[42] C. R. Anderson, K. H. Andersen, W. G. Stirling, P. E. Sokol, and R. M. Dimeo, Phys. Rev. B **65**, 174509 (2002).
[43] F. Albergamo, J. Bossy, P. Averbuch, H. Schober, and H. R. Glyde, Phys. Rev. Lett. **92**, 235301 (2004).
[44] F. Albergamo, H. R. Glyde, D. R. Daughton, N. Mulders, J. Bossy, and H. Schober, Phys. Rev. B **69**, 014514 (2004).
[45] S. Moroni and M. Boninsegni, J. Low Temp. Phys. **136**, 129 (2004).
[46] D. E. Galli and L. Reatto, Phys. Rev. Lett. **96**, 165301 (2006).
[47] B. Coasne, S. K. Jain, and K. E. Gubbins, Phys. Rev. Lett. **97**, 105702 (2006).
[48] E. H. Graf, V. J. Minkiewicz, H. Bjerrum Moller, and L. Passell, Phys. Rev. A **10**, 1748 (1974).
[49] H. R. Glyde, *Excitations in Liquid and Solid Helium* (Oxford University Press, Oxford, 1994).
[50] K. H. Andersen, W. G. Stirling, H. R. Glyde, R. T. Azuah, A. D. Taylor, S. M. Bennington, and Z. A. Bowden, Physica B **197**, 198 (1994).
[51] H. R. Glyde, M. R. Gibbs, W. G. Stirling, and M. A. Adams, Europhys. Lett. **43**, 422 (1998).
[52] J. V. Pearce, R. T. Azuah, B. Fåk, A. R. Sakhel, H. R. Glyde, and W. G. Stirling, J. Phys.: Condens. Matter **13**, 4421 (2001).
[53] N. N. Bogoliubov, J. Phys. (USSR) **11**, 23 (1947).
[54] J. Gavoret and P. Nozières, Ann. Phys. (N.Y.) **28**, 349 (1964).
[55] A. Griffin, *Excitations in a Bose Condensed Liquid* (Cambridge University Press, Cambridge, 1993).
[56] J. Bossy, J. V. Pearce, H. Schober, and H. R. Glyde, Phys. Rev. Lett. **101**, 025301 (2008).
[57] H. R. Glyde, J. V. Pearce, J. Bossy, and H. Schober, in *Recent Progress in Many Body Theories*, edited by G. E. Astrakharchik, J. Boronat, and F. Mazzanti (World Scientific, Singapore, 2008), Vol. 14, p. 401.
[58] O. Plantevin, H. R. Glyde, B. Fåk, J. Bossy, F. Albergamo, N. Mulders, and H. Schober, Phys. Rev. B **65**, 224505 (2002).
[59] F. Albergamo, J. Bossy, J. V. Pearce, H. Schober, and H. R. Glyde, Phys. Rev. B **76**, 064503 (2007).
[60] S. Miyamoto and Y. Takano, Czech. J. Phys. **46** (S1), 137 (1996).
[61] K. Huang and H.-F. Meng, Phys. Rev. Lett. **69**, 644 (1992).
[62] I. F. Herbut, Phys. Rev. B **61**, 14723 (2000).
[63] T. Roscilde and S. Haas, Phys. Rev. Lett. **95**, 207206 (2005); **99**, 047205 (2007).
[64] A. Priyadarshee, S. Chandrasekharan, J. W. Lee, and H. U. Baranger, Phys. Rev. Lett. **97**, 115703 (2006).
[65] 4F International Co., 3636 Northwest 68 Lane, Gainesville, Florida 32653.
[66] E. P. Barrett, L. G. Joyner, and P. P. Halenda, J. Am. Chem. Soc. **73**, 373 (1951).
[67] S. Brunauer, P. H. Emmett, and E. Teller, J. Am. Chem. Soc. **60**, 309 (1938).
[68] A. Corma, Q. B. Kan, M. T. Navarro, J. Perez-Pariente, and F. Rey, Chem. Mater. **9**, 2123 (1997).
[69] K. Shirahama, J. Low Temp. Phys. **146**, 485 (2007).
[70] K. Yamamoto, Y. Shibayama, and K. Shirahama, J. Low Temp. Phys. **150**, 353 (2008).
[71] D. Wallacher, M. Rheinstaedter, T. Hansen, and K. Knorr, J. Low Temp. Phys. **138**, 1013 (2005).
[72] E. Blackburn, S. K. Sinha, C. Broholm, J. R. D. Copley, R. W. Erwin, and J. M. Goodkind, arXiv:0802.3587 (unpublished).
[73] V. J. Minkiewicz, T. A. Kitchens, F. P. Lipshultz, R. Nathans, and G. Shirane, Phys. Rev. **174**, 267 (1968).
[74] M. H. Kalos, D. Levesque, and L. Verlet, Phys. Rev. A **9**, 2178 (1974).
[75] M. Rossi, D. E. Galli, and L. Reatto, Phys. Rev. B **72**, 064516 (2005).
[76] H. Godfrin, V. Lauter-Pasyuk, H. Lauter, and P. Leiderer, Institut Laue Langevin Report No. 6-01-177, 1998 (unpublished).
[77] S. A. Khairallah and D. M. Ceperley, Phys. Rev. Lett. **95**, 185301 (2005).